SSC22-P2-14

Avionics System and Attitude Algorithms for a Deorbit Device Based on an Electrodynamic Tether

Sergio Garcia-Gonzalez, Lorenzo Tarabini Castellani, Sofia Orte, Asier Ortega
Sener Aeroespacial
C. Severo Ochoa 4, 28760, Tres Cantos, Spain; +34 63 668 3104
sergio.garcia@aeroespacial.sener

Gonzalo Sanchez-Arriaga
Universidad Carlos III de Madrid
Avenida de la Universidad 30, 28911, Leganés, Spain; +34 91 624 8229
gonsanch@ing.uc3m.es

Enrico C. Lorenzini
Università degli Studi di Padova
Via Venezia 1, 35131, Padova, Italy; +39 049 827 6766
enrico.lorenzini@unipd.it

Martin Tajmar
Technische Universität Dresden
Institute of Aerospace Engineering, 01062 Dresden, Germany; +49 351 463 38125
martin.tajmar@tu-dresden.de

Katia Wätzig
Fraunhofer Institute for Ceramic Technologies and Systems
Winterbergstraße 28, 01277 Dresden, Germany; +49 351 2553-7877
katja.waetzig@ikts.fraunhofer.de

ABSTRACT

The main goal of the Electrodynamic Tether technology for PAssive Consumable-less deorbit Kit (E.T.PACK) project is to develop a deorbit device based on an electrodynamic tether with TRL 4 by 2022. In September 2022, its continuation, i.e. the E.T.PACK-F project, will carry on with the activities of E.T.PACK to prepare a flight model with TRL 8 that will be tested in an in-orbit demonstration mission in 2025. This work (i) describes the attitude determination and control strategy of the mission, which is used as a means of explaining its different phases and the dynamics of each one of them, (ii) provides a description of the avionics elements of the whole system, (iii) describes some of the tests performed until this moment, and (iv) summarizes the current status and the future work.

1. INTRODUCTION

The sustainable use of space is an important topic on the agenda of spacefaring countries since the space debris population is already under the Kessler syndrome [1]. The density of objects in low-Earth orbits increases every year due to the appearance of mega-constellations and the so-called "new space" [2, 3]. A scenario with cheaper launchers and less reliable satellites is foreseen. A deorbiting device would find a place in the emerging market of in-orbit servicing, providing that it is reliable, light, and cost-effective. In this scenario, space ElectroDynamic Tethers (EDTs) appear as a promising candidate for deorbiting space debris, due to their passive and propellant-less nature.

Deorbit technologies can be classified as active or passive. Active technologies, including chemical and electrical propulsion, have been traditionally used. However, they are limited by the amount of propellant available on board. Nowadays, passive strategies have gained strength, motivated by the space debris problem, due to their propellant-less nature Among them, a deorbit device based on an EDT could be a game-changer in the deorbiting market given that i) it can operate in thrust or drag mode [4], (ii) it can be lighter than other active and passive strategies [6], (iii) controlled re-entry of spacecraft below around 1 ton is not necessary because they are completely burned during their passes through the atmosphere, and (iv) it can be fitted into a compact,

low-cost, autonomous deorbit device. This last statement represents the main goal of the E.T.PACK project [5].

A tether of length L moving at a relative velocity $\boldsymbol{v}_{rel}$ with respect to the Earth's magnetic field, $\boldsymbol{B}$, generates an electric field $\boldsymbol{E} = \boldsymbol{v}_{rel} \times \boldsymbol{B}$ at the faraway plasma [7]. If there is good contact between the tether and the plasma, a steady electrical current $\boldsymbol{I}$ flows through the tether. In the presence of the external magnetic field, the Lorentz force appears, $\boldsymbol{F}_L = \int_0^L \boldsymbol{I}(s) \times \boldsymbol{B}\, ds$, that can be used as thrust or drag. Using this operation principle, the goal of the E.T.PACK-F deorbit device is to deorbit itself from a circular 600 km orbit in less than 100 days.

E.T.PACK is a FET-open project (Horizon2020) that started in 2019 and found continuity with the EIC Innovation project entitled "A Ready-to-Fly Deorbit Device Based on Electrodynamic Tether Technology" (E.T.PACK-F). Funded with a total of 5.5 M€ by the European Commission, the main objective of E.T.PACK and E.T.PACK-F is to develop and qualify a prototype of a 12U deorbit device based on a 500 m EDT by 2025. The mentioned device is composed of two modules, mechanically connected during launch, that will separate in orbit while deploying 500 m of tether.

The purpose of this article is to provide a general overview of the In-Orbit Demonstration (IOD) mission, paying special attention to its ADCS and avionics. ADCS algorithms are not fully described here, but their main results are summarized, and useful references with the details are provided. The work is organized as follows. Section 2 provides a general overview of the demonstration mission and the deorbit device. The ADCS strategy is summarized in Section 3 for each one of the three phases in which the mission can be divided. Section 4 describes the avionics elements of each module. In Section 5, some of the tests performed until now are summarized. Finally, in Section 6, some conclusions about the current status and future work are given.

2. MISSION DESCRIPTION

The E.T.PACK deorbit device has been designed to fit into a standard 12U envelope, with a maximum mass of 24 kg. It is composed of two modules: the Deployment Mechanism Module (DMM), with an approximated dimension of 2U x 2U x 1.5U, and the Electron Emitter Module (EEM), with 2U x 2U x 2.5U of rough size, see Figure 1. The former hosts 500 m of tape-tether (80% Aluminum and 20% PEEK) and it is responsible for deploying it. The latter's main goals are (i) to emit the electrons captured by the tether back to the ambient plasma to maintain a steady electrical current in the tether, (ii) to activate the Hold Down and Release Mechanism (HDRM) before the tether deployment to break the mechanical connection between it and the DMM, and (iii) provide the necessary acceleration during the deployment phase. The avionics of both modules is similar, with some differences that correspond to the dedicated electronics of the deployment mechanism in the DMM and the electron emitter in the EEM.

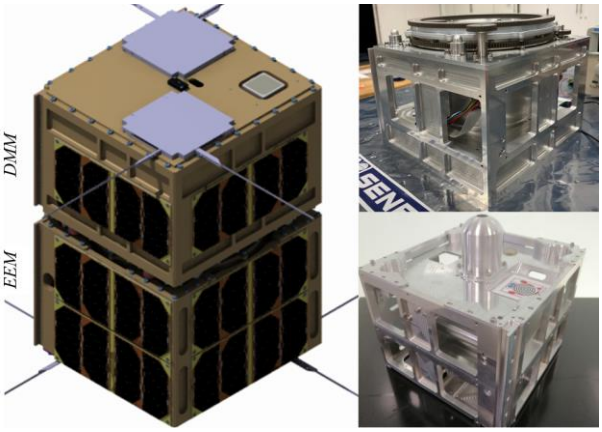

Figure 1: 3D model of the E.T.PACK deorbit device and manufactured structures of each module (DMM and EMM).

The main objective of the IOD is deorbiting the whole system from a circular orbit of 600 km of altitude and mid-inclination in less than 100 days. In the IOD, the deorbit device will be on its own, that is, it will not be attached to any other body (e.g., a bigger spacecraft or the last stage of a launcher). However, after a successful proof of concept, this deorbit device will be the base of a commercial product able to deorbit an uncooperative piece of space debris of up to 1 ton.

The IOD is divided into three main phases:

- *Pre-deployment:* Its main goal is to detumble and point the deorbit device to a specific direction, which will be the initial condition for the deployment. In this phase, both modules are mechanically attached.
- *Deployment:* the deployment of the tether will be performed aided by the deployment mechanism and two cold gas systems. With a duration of 3600 s, it is the critical phase of the mission.
- *Deorbiting:* It starts after the deployment and lasts until the disintegration of the deorbit device in the atmosphere. The altitude of the orbit decreases thanks to the force provided by the Lorentz drag.

The three main phases of the mission are described in detail in Section 3, along with the ADCS algorithms.

3. ADCS

The design of the attitude determination and control strategy of a space tether mission represents a challenge due to the very different dynamics that the system experiences in each of the three previously described stages. The main goal is to be able to fulfill the requirements in each case with the same set of actuators. Each module is equipped with a set of three mutually orthogonal magnetorquers and a cold-gas system, which is only available after the deployment phase. The use of reaction wheels has been avoided due to a cost requirement. An Extended Kalman Filter (EKF) is used during the whole mission, regardless of the phase, to estimate the attitude of each module.

Extended Kalman Filter (EKF)

The implemented filter is a multiplicative EKF fed by a low-cost gyroscope, a magnetometer, a set of coarse Sun sensors, and a GNSS sensor. The basic idea behind multiplicative filters is to use the quaternion as the "global" attitude representation and use a three-component state vector (e.g., the rotation vector $\delta\boldsymbol{\vartheta}$) for the "local" representation of attitude errors [8]. The filter writes the true quaternion ($\boldsymbol{q}$) and bias vector of the gyro ($\boldsymbol{\beta}_G$) as a function of their estimation ($\widehat{\boldsymbol{q}}$ and $\widehat{\boldsymbol{\beta}}_G$) and errors ($\delta\boldsymbol{q}$ and $\Delta\boldsymbol{\beta}_G$) as follows

$$\boldsymbol{q} = \delta\boldsymbol{q}(\delta\boldsymbol{\vartheta}) \otimes \widehat{\boldsymbol{q}}, \tag{1}$$

$$\boldsymbol{\beta}_G = \widehat{\boldsymbol{\beta}}_G + \Delta\boldsymbol{\beta}_G, \tag{2}$$

where $\delta\boldsymbol{\vartheta}$ represents the attitude error between the estimation and the reality, $\Delta\boldsymbol{\beta}_G$ does the same for the gyro bias vector, and the operator $\otimes$ is used to represent the quaternion multiplication [8]. The error quaternion $\delta\boldsymbol{q}$ used in Eq. (1) is expressed as a function of the rotation vector $\delta\boldsymbol{\vartheta}$ [9]. The filter's objective is to estimate $\delta\boldsymbol{\vartheta}$ and $\Delta\boldsymbol{\beta}_G$, which form the EKF state vector. These two vectors can be understood as the "local" representation of attitude errors that modify the values of the "global" representation, given in Eqs. (1) and (2), in each iteration of the filter. After this "transfer" of knowledge from the local to the global representation is performed, a reset process sets to zero the values of $\delta\boldsymbol{\vartheta}$ and $\Delta\boldsymbol{\beta}_G$ for the next iteration. The measurement vector of the EKF includes the normalized Earth's magnetic field direction, obtained from the magnetometer, and the normalized Sun direction, obtained by the set of coarse Sun sensors. The mathematical details of this filter are not described in this section, which is intended to serve as a summary. A thorough description of this filter is in Refs. [8, 9, 10].

The main advantages of this filter are:

- *The low dimension of the state vector:* Thanks to this dual representation of the attitude variables, the state vector of the filter has a dimension equal to six. This feature makes it especially suitable to be embedded in an on board computer for real-time operations.
- *Direct interpretation of the covariance matrix:* Unlike other filters, the covariance matrix has a very clear interpretation. Its diagonal terms represent the variance of the error between estimation and reality.
- *Existence of an exact discrete formulation:* To implement any EKF in a digital computer, a discretization process must be performed. Usually, it involves the approximation of the state-transition matrix [11]. In the selected EKF, Maclaurin series of sines and cosines can be recognized in the state-transition matrix expression [10]. Therefore, no approximation is made, resulting in an exact discretization of the filter.

In the EKF, we adopt the "gyros for dynamic model replacement" [8], which avoid the use of a dynamical model and, hence, knowledge of the inertia tensors of the modules. This is particularly useful in our case since the inertia tensors differ strongly from one phase of the mission to another.

It must be highlighted that the EKF is running on both modules during the three phases. Although during the pre-deployment phase both modules are still mechanically attached and, hence, only one EKF is necessary, both modules will run their respective EKF to reach the convergence before the deployment phase.

In Ref. [9], the EKF was subjected to several Monte Carlo analyses to assess its performance against different errors in the attitude sensors. Cases with unconsidered biases ($\boldsymbol{\beta}$), gain factors ($\boldsymbol{K}$), and misalignments ($\boldsymbol{\Delta}$) in the gyroscope and magnetometer were analyzed. The sun vector, obtained thanks to the different inputs from the set of coarse Sun sensors, was modeled as a high noise input available only during daylight conditions. The performance of the EKF under the previous errors is summarized in Table 1, which has been adapted from Ref. [9]. Each Monte Caro analysis includes 20 shots, varying the initial conditions of the deorbit device. The figures of merit $\overline{\delta\vartheta}$ and $\sigma_{\delta\vartheta}$ represent the average value of $\delta\vartheta$ and its standard deviation, respectively, during 3 orbits.

In the absence of any unaccounted error, the EKF has an average error of 0.12 ± 0.05 deg in daylight conditions and 0.17 ± 0.09 deg in eclipse conditions. The most critical error parameter is the magnetometer bias,

especially during eclipse conditions. The effect of the magnetometer gain factor is almost negligible since the filter uses the normalized vector of the Earth's magnetic field. Therefore, any gain factor in the magnetometer is softened by this normalization process. The rest of parameters ($\boldsymbol{\Delta}_M$, $\boldsymbol{K}_G$, and $\boldsymbol{\Delta}_G$) have a small influence. In any case, the EKF satisfies comfortably the determination requirements of the mission. Figure 2 shows the attitude error between estimation and reality ($|\delta\boldsymbol{\vartheta}|$) during 3 orbits for different values of the magnetometer bias.

Table 1: Performance [deg] of the EKF under the presence of unaccounted errors in the attitude sensors. The subscripts M and G refer to the magnetometer and gyroscope, respectively.

$\|\boldsymbol{\beta}_M\|$	$\mathbf{0.25\ \mu T}$	$\mathbf{0.5\ \mu T}$	$\mathbf{1\ \mu T}$
$\overline{\delta\vartheta} \pm \sigma_{\delta\vartheta}\|_{day}$	0.20 ± 0.09	0.33 ± 0.18	0.62 ± 0.36
$\overline{\delta\vartheta} \pm \sigma_{\delta\vartheta}\|_{eclip}$	0.34 ± 0.15	0.60 ± 0.23	1.16 ± 0.43
$\|\boldsymbol{K}_M\|$	$\mathbf{2 \cdot 10^{-3}}$	$\mathbf{4 \cdot 10^{-3}}$	$\mathbf{8 \cdot 10^{-3}}$
$\overline{\delta\vartheta} \pm \sigma_{\delta\vartheta}\|_{day}$	0.12 ± 0.05	0.12 ± 0.05	0.13 ± 0.06
$\overline{\delta\vartheta} \pm \sigma_{\delta\vartheta}\|_{eclip}$	0.17 ± 0.09	0.18 ± 0.09	0.19 ± 0.09
$\|\boldsymbol{\Delta}_M\|$	$\mathbf{2 \cdot 10^{-3}}$	$\mathbf{4 \cdot 10^{-3}}$	$\mathbf{8 \cdot 10^{-3}}$
$\overline{\delta\vartheta} \pm \sigma_{\delta\vartheta}\|_{day}$	0.13 ± 0.06	0.14 ± 0.06	0.20 ± 0.09
$\overline{\delta\vartheta} \pm \sigma_{\delta\vartheta}\|_{eclip}$	0.19 ± 0.09	0.22 ± 0.10	0.33 ± 0.14
$\|\boldsymbol{K}_G\|$	$\mathbf{2 \cdot 10^{-3}}$	$\mathbf{4 \cdot 10^{-3}}$	$\mathbf{8 \cdot 10^{-3}}$
$\overline{\delta\vartheta} \pm \sigma_{\delta\vartheta}\|_{day}$	0.13 ± 0.06	0.14 ± 0.06	0.19 ± 0.08
$\overline{\delta\vartheta} \pm \sigma_{\delta\vartheta}\|_{eclip}$	0.18 ± 0.09	0.22 ± 0.11	0.32 ± 0.15
$\|\boldsymbol{\Delta}_G\|$	$\mathbf{2 \cdot 10^{-3}}$	$\mathbf{4 \cdot 10^{-3}}$	$\mathbf{8 \cdot 10^{-3}}$
$\overline{\delta\vartheta} \pm \sigma_{\delta\vartheta}\|_{day}$	0.13 ± 0.06	0.15 ± 0.07	0.22 ± 0.09
$\overline{\delta\vartheta} \pm \sigma_{\delta\vartheta}\|_{eclip}$	0.19 ± 0.10	0.24 ± 0.12	0.37 ± 0.17

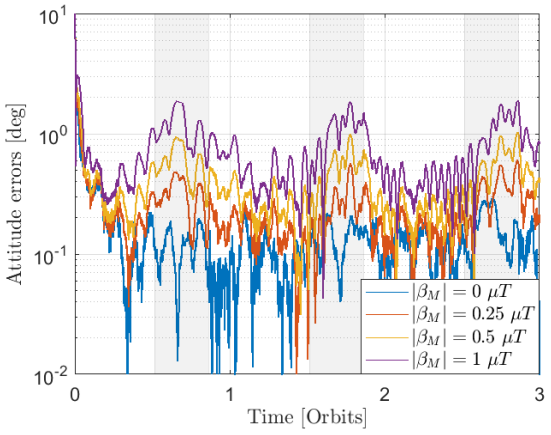

Figure 2: Evolution of the EKF attitude determination error for different values of unaccounted magnetometer bias. Gray zones are used to represent eclipse periods.

Pre-deployment phase

The pre-deployment phase starts after the orbital injection and lasts until right before the deployment of the tether system. During this phase, the HDRM still holds mechanically both modules. Therefore, they act like a single rigid body. The main goals of this phase are:

- Detumbling of any unwanted angular velocity of the deorbit device.
- 3-axis attitude pointing to align the deorbit device longitudinal axis with a fixed direction within the orbital frame (15 deg deviated from the zenith direction) [9].

No module has available its cold-gas system during this phase given that the thrusters are covered by the other module (see Figures Figure 1 and Figure 4). Therefore, both goals must be fulfilled with magnetic actuation only. In Ref. [9], a method to accomplish this goal is presented. The module in charge of commanding its magnetorquers to satisfy the requirements of this phase is the EEM.

The detumbling control law is [8]

$$\boldsymbol{m} = \frac{k}{|\boldsymbol{B}|^2}\boldsymbol{\omega}_{BI} \times \boldsymbol{B}, \tag{3}$$

where $\boldsymbol{m}$ represents the magnetic dipole to be commanded by the magnetorquers, $\boldsymbol{B}$ is the Earth's magnetic field, $\boldsymbol{\omega}_{BI}$ is the angular velocity of the deorbit device with respect to the inertial frame, and k is a positive gain. As pointed out in Ref. [9], the optimum value of k is around 10^{-3} for which the deorbit device is able to detumble from an initial angular velocity of $0.4\ \mathrm{rad/s}$ to $0.01\ \mathrm{rad/s}$ in roughly one orbit.

Once the initial unwanted angular velocity has been removed, the longitudinal axis of the deorbit device must be pointed to the "deployment direction" with a minimum accuracy of 10 deg. The deployment direction is contained within the orbital plane, and it is obtained after performing a 15 deg rotation of the deorbit device position vector (see Ref. [9] for a detailed definition). The deployment direction represents the initial condition for the deployment phase, and it is important for the stability of the deployment maneuver [12]. The method proposed for achieving this attitude is based on the following control law [9]

$$\boldsymbol{m} = \boldsymbol{B} \times (-\boldsymbol{K}\boldsymbol{x} + \boldsymbol{u}), \tag{4}$$

where $\boldsymbol{x}$ is the state vector of the system (defined as a function of the quaternion vector of the deorbit device

frame with respect to the orbital frame), $\boldsymbol{K}$ is a control gain obtained by the LQR method, and $\boldsymbol{u}$ is a secular term. The suitability of this control law has been verified by Monte Carlo analysis [9]. It revealed that the value of the unaccounted residual magnetic dipole of the deorbit device is the most critical parameter. Depending on this value, the maximum pointing accuracy requirement (10 deg) is achieved during 80%, 74%, 55%, and 22% of the orbit, on average, for an unknown residual magnetic dipole of 0, 2, 4, and 8 $\mathrm{mA \cdot m^2}$.

Deployment phase

The deployment phase is the critical phase of the mission. In a 1-hour maneuver, the DMM and EEM must coordinate their actions to deploy 500 m of tether while separating from each other with the right acceleration profile. Details of the deployment maneuver can be found in Ref. [12]. The attitude of each module is controlled during the whole phase. It is especially important in the DMM module since it is the one that contains the deployment mechanism. An uncontrolled attitude could cause the entanglement of the tether around the modules, which would jeopardize the entire deployment maneuver. Each module counts on a cold-gas system as well as the set of attitude sensors described before.

Figure 3: Artistic representation of deorbit device during the deployment phase.

Once the deorbit device acquires the right attitude, the HDRM breaks the mechanical connection between both modules, which are at that moment only connected by the tether (see Figure 3). For 30 seconds, the EEM activates its cold-gas system to provide the right acceleration profile. At the same time, the DMM starts to command the deployment mechanism to release the EDT. This is referred to as the "acceleration phase". During the entire deployment, each module controls its attitude thanks to a cold-gas system and the previously described EKF. There are four thrusters, all of them located on the same face for each module (see Figure 4 for the EEM case). When the HDRM is still active, the cold-gas systems are unavailable since all their thrusters are covered by the other module. The objective of the attitude control is to point the longitudinal axis of each module in the direction of the tension force. The angle between these two vectors (α) is one of the main figures of merit of this phase.

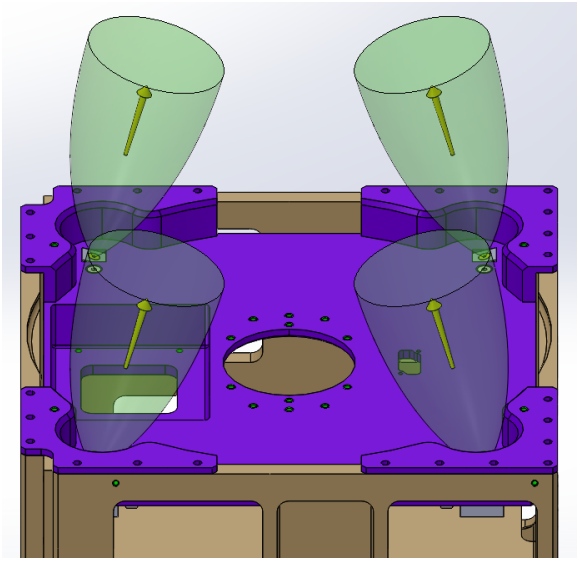

Figure 4: EEM cold-gas system thrusters' locations.

The implementation of an ADCS scheme for the deployment phase represents a challenge due to the complex dynamics of the maneuver. The tether was modeled as a single spring-dashpot system of varying stiffness and damping coefficient, according to the amount of Aluminum and PEEK ejected at each moment. The tether is connected to the four corners of the EEM, the corners of the face shown in Figure 4, and to the deployment mechanism in the DMM. The DMM deployment mechanism performs a circular rotation around its longitudinal axis. Therefore, unlike the EEM, there is a varying offset between the tether attachment point and the center of the deployment mechanism face. This issue complicates the DMM attitude control, but it has many advantages regarding the internal functioning of the deployment mechanism. Therefore, the control must overcome this difficulty. The attitude dynamics of both modules are coupled by the EDT. Thermal effects are also present, although they are not so relevant in this maneuver.

There are two parameters that have an important effect on the attitude control of both modules during this phase:

- The stiffness of the tether.
- The separation between the DMM longitudinal axis and the tether attachment point.

Regarding the former and to facilitate the deployment maneuver, an In-Line Damper (ILD) [13] was included in the tether with the objective of reducing its stiffness. Currently, a stiffness value of roughly 5 N/m is considered in the design. Concerning the latter, a non-zero distance between the DMM longitudinal axis and the tether extraction point causes time-varying non-longitudinal components of the extraction point vector (in the DMM body frame) due to its rotating movement during the deployment phase. If this distance is sizeable, these components will induce tension peaks that will perturb the attitude of both modules. Effort has been made to reduce this distance. Currently, it is equal to 55 mm but it will be reduced to 45 mm in the next version of the deployment mechanism.

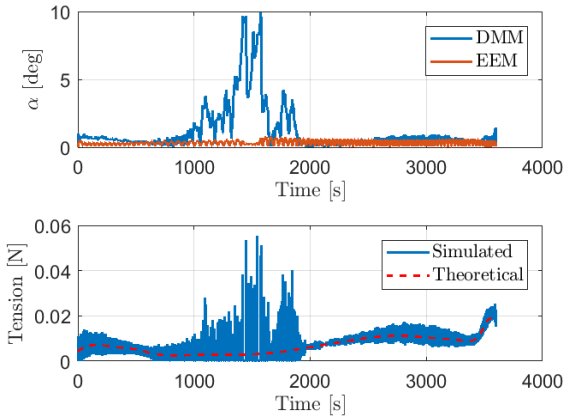

Figure 5: Angular deviation between the longitudinal axis of each module and the tension force (top) and tension profile experienced by each module (bottom).

The control law for the restoring torque is based on a Proportional-Derivative (PD) scheme which involves the attitude and angular velocity of each module, as well as the tension force. This control scheme is Sener Aeroespacial proprietary and its details cannot be disclosed. However, its performance is shown in Figure 5. In general, the values of α in the DMM are bigger than those of the EEM since the tether is only connected to the DMM at a single moving point, while the EEM possesses four attachment points (at its four corners) in the so-called sub-tether configuration [14]. The results of the simulation have been compared with another set of simulations based on a simplified model [12]. In the latter, the dynamics is constrained in the orbital plane and both modules are modelled as points. The simulated tension profile of the detailed simulation oscillates around the one obtained in the 2D analysis. The amplitude of these oscillations is directly proportional to the tether stiffness and the horizontal distance between the DMM longitudinal axis and the tether attachment point. This is the reason why these parameters are crucial for the deployment maneuver.

Deorbiting phase

The deorbiting phase is the longest phase of the mission. It starts after the tether deployment and lasts until the disintegration of the deorbit device in the upper layers of the atmosphere. At this stage, all tether segments have been deployed and, hence, the tether length is constant. The Lorentz drag is present during the whole phase thanks to the passive capture of electrons by the bare segment of the EDT and their emission at the electron emitter. These two phenomena are responsible for maintaining a steady electrical current along the EDT that, in the presence of the Earth's magnetic field, generates the Lorentz drag. According to our simulations, the E.T.PACK deorbit device should be able to deorbit itself from a mid-inclination 600 km orbit in roughly 35 days if the electron emitter is always on.

The ADCS goal during this phase is to avoid large oscillations in the modules that could cause the entanglement of the tether around different parts of the structure and the antennas or the generation of electrical arcs. Special care must be taken at the transitions from daylight to eclipse and vice versa. The high thermal expansion coefficient of Aluminum along with its large exposure area makes it especially sensitive to thermal changes in its environment, as shown in Figure 6. During these transitions, the tether shrinks and expands up to 2.5 meters, roughly, which induces tension peaks and tension slackness. This effect is shown in Figure 6, which displays a fraction of an orbital period (3000 seconds).

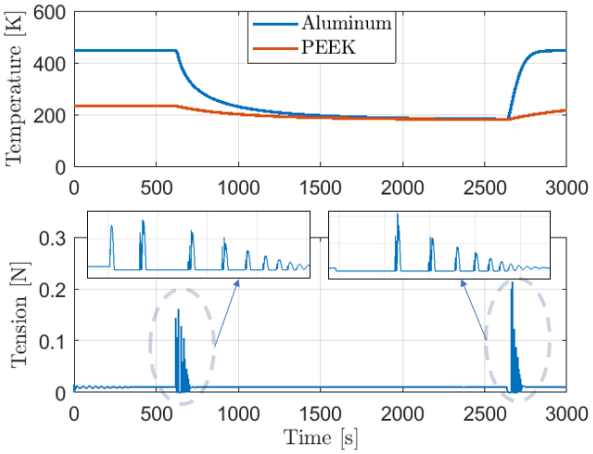

Figure 6: Thermal evolution of the tether (top) and tension profile (bottom) during the first 3000 seconds of an orbit.

The control law given in Eq. (3) is used during this phase to keep the angular momentum of each module at its

minimum. With this strategy, we are able to (i) reduce the amplitude of the oscillations during these transitions and (ii) damp them. It also meets the requirement imposed on each module, which is to keep the α angle below 90 degrees.

4. AVIONICS

The avionics of both modules is similar because both modules have mainly the same requirements in terms of ADCS, communication, power consumption, etc. Only the dedicated electronics intended to control the deployment mechanism, in the DMM, and the electron emitter, in the EEM, introduce variations between both systems. In this work, we will not focus on these differences, instead, we will provide a general description of the shared elements, which are shown in Figure 7.

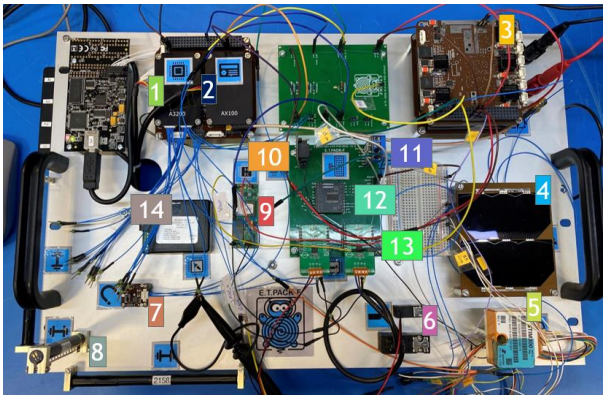

Figure 7: Current status of the deorbit device flatsat: (1) OBC, (2) TMTC radio, (3) EPS, (4) Solar panel, (5) IMU, (6) Shut-off valves, (7) Magnetometer, (8) Magnetorquers, (9) DCDC converter, (10) Logic level converter, (11) RS422 to RS232 converter, (12) GPIO expander, (13) H-bridges, and (14) Thrusters drivers.

Currently, two different alternatives for the on board computer (OBC) have been considered and tested: a powerful System on Chip consisting of an ARM processor plus an FPGA (Zynq-7000 [15]) and a commercial space-qualified AV32 microprocessor [16]. The former has been implemented in the DMM module for the testing of the deployment mechanism. In this architecture, the FPGA is in charge of handling the communication with all sensors and actuators, freeing the CPU from these time-consuming tasks. The CPU implements the NASA core Flight System (cFS) platform, which is based on the idea of reusing pieces of software to minimize the required manpower to develop space flight software applications. It also possesses many other advantages, that can be found in Ref. [17]. In this strategy, summarized in Figure 8 (a), the different applications (i.e., threads) such as the scheduler, housekeeping, ground request, ADCS, etc. run in parallel on the ARM. Whenever one of these applications needs to interact with a sensor/actuator, it uses the FPGA as an interface. The FPGA is also responsible for reading data periodically from the available sensors and saving this information in memory. The second alternative, based on the AV32 chip, represents the traditional software approach in which a single micro is in charge of running the different parts of the software and also interacting with all sensors and actuators. This architecture is summarized in Figure 8 (b). The micro with this second alternative is the one shown in Figure 7. A comparison between both strategies is provided in Table 2.

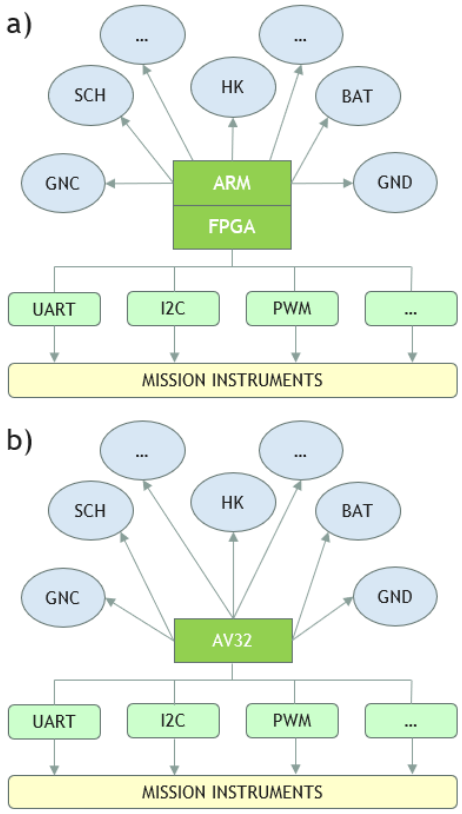

Figure 8: Differences between the two software architectures. (a) refers to the ARM(cFS)+FPGA strategy and (b) refers to the traditional software approach with an AV32 micro.

Table 2: Comparison between the two different software architectures.

ARM+FPGA	AV32
Capable of handling high-frequency sensors and actuators	Not able to handle high-frequency sensors and actuators
The flight heritage is not high	High flight heritage
Different functionalities (I/O pins, PWM, etc.) can be added for each specific application. The design is alive and can change depending on the case	Unique design. If some elements are missing (such as more I/O pins or more PWM channels), extra circuitry must be added

Very powerful resources (large memories, high clock frequency, interfaces, etc.)	Adequate resources (memories, clock speed, interfaces, etc.)
Operating system: Petalinux	Operating system: FreeRTOS
Needs software and firmware knowledge	Only needs software knowledge
It does not include additional elements	Includes additional sensors and drivers
Higher form factor	Lower form factor
Higher power consumption	Lower power consumption

The final decision will be made after the conclusion of the E.T.PACK project (November 2022) and it will be based mainly on the capability to successfully command all the hardware, the state of maturity, type of manpower required to program it, and company interests, among others.

The TeleMetry and TeleCommand (TMTC) system is based on a half-duplex UHF transceiver. Both modules must be able to interact independently with the ground station. Therefore, each one of them includes its own radio. The communication protocol is based on the cubesat space protocol (csp) [18]. This protocol is intended to be used in a small network, easing the communication among different nodes (e.g., a satellite and different ground stations). It is based on a 32-bit header containing information from the network.

Both modules count on different attitude sensors: a magnetometer, a set of coarse Sun sensors and an inertial measurement unit (IMU), and attitude actuators: three magnetometers and a cold-gas system. The magnetometer must be placed far away from any magnetic perturbance. Its final location is subjected to the results of magnetic tests. The coarse Sun sensors are placed on the solar panels, present on all the external faces of each module. The IMU is the key element of the EKF. It possesses a serial differential communication protocol (RS422) that makes it especially suitable for high-noise applications. Its data must be converted to RS232 to be read by the OBC. Concerning the attitude actuators, the three magnetometers are controlled using the Power-Width Modulation (PWM) technique by the OBC. Three H-bridges are needed to change the sense of the current. Finally, the cold-gas system uses two types of 24 V shut-off valves, that can be controlled by employing H-bridges, relays, or switches, and the thrusters' valves. The drivers of the thrusters are of spike-and-hold type and are controlled using 5V TTL signals coming from the OBC. Given that the OBC only works at 3.3 V level, all these signals must go through a logic level converter first.

Each module includes an Electrical Power Subsystem (EPS) to provide energy to the elements. The EPS can store, convert, and distribute the energy that comes from the solar panels. Its capacity is equal to 38.5 Wh and it is composed of four 2.6 mAh Li-Ion cells in series. Although the EPS has several internal DCDC converters to provide voltage lines of 5 and 3.3 V, an additional DCDC converter must be added to provide a stable 24 V line for the operation of the deployment mechanism, electron emitter, and the shut-off valves.

5. TESTS

Tests of a very different nature have been performed at this stage of the project. Some of the most relevant ones are listed below:

- *Open-loop tests of the ADCS algorithms*: The EKF and control laws described in Section 3 have been autocodified and embedded into the OBC. The open-loop tests consist of checking that the outcomes of these algorithms, when running on the OBC, is the same (or very similar) as the output of the same algorithms when they were running on the simulator.
- *Tether deployment tests*: The deployment mechanism has been tested several times, showing a very good performance. The different motors of this mechanism must be commanded independently to extract the tether.
- *Avionics tests*: Electrical tests have been performed on the avionics described in Section 4 to ensure the correct behavior of all the procured sensors and actuators, the correct implementation of their drivers into the OBC, and to check that all the different equipment can coexist in a noiseless environment.
- *Communication tests*: A ground station simulator, has been developed for checking the right transmission and reception of data to/from the ground station. Instead of UHF, a CAN interface has been used for transmitting the data in both directions. Different commands have been created to modify the configuration parameters of the satellite or request data (e.g., "start deployment maneuver" or "send housekeeping").

6. CONCLUSIONS

This work presented the status of the avionic system and the ADCS algorithms of the deorbit device that is currently under development in the framework of the E.T.PACK project. The different phases of the mission have been studied through numerical simulation. Regarding ADCS, the importance of the residual magnetic dipole has been highlighted. Accurate knowledge of this variable is necessary for the future mission. Also, the stiffness of the ILD must be reduced

as much as possible to ease the deployment maneuver. Concerning the avionics, the work presented the elements on-board the two modules of the deorbit device. The proposed architecture fits into the tough volume, mass, and power enveloped posed by the two modules of the deorbit device.

Acknowledgements

Garcia-Gonzalez's work was supported by Comunidad de Madrid (Industrial PhD with grant number IND2019/TIC17198). Additionally, this work was supported by the European Unions Horizon 2020 Research and Innovation Programme under grant agreement No 828902 (E.T.PACK project).

References

1. D.J. Kessler and B.G. Cour-Palais, "The creation of a debris belt," Journal of Geophysical Research, 83 (A7), pp. 2637-2646, 1978.
2. S. Le May, S. Gehly, B.A. Carter, and S. Flegel, "Space debris collision probability analysis for proposed global broadband constellations," Acta Astronautica, 151, pp. 445-455, 2018.
3. J. Radtke, C. Kebschull, and E. Stoll, "Interactions of the space debris environment with mega constellations - Using the example of the OneWeb constellation," Acta Astronautica, 131, pp. 55-68, 2017.
4. J.R. Sanmartin, M. Martinez-Sanchez, and E. Ahedo, "Bare Wire Anodes for Electrodynamic Tethers," Journal of Propulsion and Power, 9(3), pp. 353-360, 1993.
5. G. Sanchez-Arriaga, S. Naghdi, K. Watzig, J. Schilm, E.C. Lorenzini, M. Tajmar, E. Urgoiti, L. Tarabini, J.F. Plaza, and A. Post, "The E.T.PACK project: Towards a fully passive and consumable-less deorbit kit based on low-work-function tether technology," Acta Astronautica, 177, pp. 821-827, 2020.
6. G. Sanchez-Arriaga, J.R. Sanmartin, and E.C. Lorenzini, "Comparison of technologies for deorbiting spacecraft from low-earth-orbit at end of mission," Acta Astronautica, 138, pp. 536-542, 2017.
7. S.D. Drell, H.M. Foley, and M.A. Ruderman, "Drag and propulsion of large satellites in the ionosphere; an alfvén propulsion engine in space," Physics Review Letter, 14, pp. 171-175, 1965.
8. F. Landis Markley and J.L. Crassidis, "Fundamentals of spacecraft attitude determination and control," Springer, 2014.
9. S. Garcia-Gonzalez and G. Sanchez-Arriaga, "Attitude Determination and Control for the Deployment Preparation Phase of a Space Tether Mission," Acta Astronautica, 193, pp. 381-394, 2022.
10. J.L. Crassidis and J.L. Junkins, "Optimal estimation of dynamics systems," Chapman Hall/CRC, 2004.
11. D. Simon, "Optimal state estimation," Willey, 2006.
12. G. Sarego, L. Olivieri, A. Valmorbida, A. Brunello, E. Lorenzini, L. Tarabini Castellani, E. Urgoiti, A. Ortega, G. Bordeles-Motta, G. Sanchez-Arriaga, "Deployment requirements for deorbiting eletrodynamic tether technology," CEAS Space Journal, 13, pp. 567-581, 2021.
13. L. Olivieri, A. Brunello, G. Sarego, A. Valmorbida, and E.C. Lorenzini, "An in-line damper for tethers-in-space oscillations dissipation," Acta Astronautica, 189, pp. 559-566, 2021.
14. K. Hovel and S. Ulrich, "Postcapture dynamics and experimental validation of subtethered space debris," Journal of Guidance, Control, and Dynamics, 41(2), pp. 519-525, 2015.
15. MicroZed Zynq hardware user guide v. 1.7, https://www.avnet.com/wps/wcm/connect/onesite/58eaef36-f0b2-4dd4-8440-540bdc2acd3d/5276-MicroZed-HW-UG-v1-7-V1.pdf?MOD=AJPERES&CACHEID=ROOTWORKSPACE.Z18_NA5A1I41L0ICD0ABNDMDDG0000-58eaef36-f0b2-4dd4-8440-540bdc2acd3d-nNnX57
16. NanoMind A3200 datasheet v. 1.17, https://gomspace.com/UserFiles/Subsystems/datasheet/gs-ds-nanomind-a3200_1006901-117.pdf
17. Core Flight System (cFS) background and overview, NASA, https://cfs.gsfc.nasa.gov/cFS-OviewBGSlideDeck-ExportControl-Final.pdf
18. CSP repository, https://github.com/libcsp/libcsp